MASKAY

Presentación

El Departamento de Eléctrica y Electrónica de la Universidad de las Fuerzas Armadas ESPE, consciente de su gran responsabilidad con la sociedad, busca proponer e impulsar iniciativas tendientes a fomentar el desarrollo integral de la ingeniería eléctrica y electrónica en el Ecuador. Como resultado de este compromiso, nace en el año 2011 la revista Maskay. Esta revista sintetiza de una forma documentada los esfuerzos en investigación y desarrollo que desarrollan los docentes/investigadores y estudiantes de la región.

En la actualidad, la revista MASKAY se encuentra indexada en diversas bases de datos: **SciELO-Ecuador**, **Latindex catálogo v2.0**, **LatAm-Studies** Estudios Latinoamericanos, **RootIndexing**, **MIAR** (Matriz de Información para el análisis de Revistas), **DOAJ** (Directory of Open Access Journals), **DRJI** Directory of Research Journals Indexing), **Dialnet** y **REDIB** (Red Iberoamericana de Innovación y Conocimiento Científico), con el objetivo de difundir a nivel internacional las publicaciones realizadas en esta revista. Además, para que exista una mejor divulgación de sus contenidos, la revista MASKAY cuenta con número **DOI (Digital Object Identifier)** legítimamente registrado y validado por **Crossref**, lo que permite una fácil localización de sus contenidos en la web.

Diego Arcos Avilés
Editor General

Presentation

The Department of Electrical, Electronics, and Telecommunications Engineering of the Universidad de las Fuerzas Armadas ESPE, aware of its great responsibility to society, seeks to propose and promote initiatives to foster the comprehensive development of electrical and electronic engineering in Ecuador. As a result of this commitment, the Maskay Journal was born in 2011. This journal presents the research and development efforts carried out by the region's teachers/researchers and students.

Currently, the MASKAY Journal is indexed in several databases: **SciELO-Ecuador**, **Latindex catalog v2.0**, **LatAm-Studies** Estudios Latinoamericanos, **RootIndexing**, **MIAR** (Information Matrix for the Analysis of Journals), **DOAJ** (Directory of Open Access Journals), **DRJI** Directory of Research Journals Indexing), **Dialnet** and **REDIB** (Ibero-American Network of Innovation and Scientific Knowledge), to disseminate the publications in this journal internationally. In addition, to better disseminate its contents, the MASKAY Journal has a **DOI (Digital Object Identifier)** number legitimately registered and validated by **Crossref**, which allows easy location of its contents on the web.

Diego Arcos Avilés
Editor-in-Chief

Contenido / Table of Contents

Biometric System: Study of Radiation on the Human Arm

Sistema Biométrico: Estudio de la radiación en el brazo humano

Jenny Cruz, Alex Ñaupa, and Belen Silva

Abstract—**The study assessed radiation power absorption in the 1.5 to 5 GHz range for Wi-Fi, LTE, and AM modulation, using three Vivaldi antennas in an anechoic chamber with a phantom arm made of animal bone, ballistic gel, and pigskin. Wi-Fi showed the highest absorption levels, but these values (0.168 mW and 0.050 mW) were below ICNIRP safety limits, indicating no significant risk to human health.**

Index Terms—**Power absorption, Wi-Fi, LTE, AM modulation, SAR, ICNIRP 2020.**

Resumen—**El estudio examinó la absorción de potencia de radiación en el espectro de 1.5 a 5 GHz para tecnologías como Wi-Fi, LTE y modulación AM, utilizando tres antenas Vivaldi en una cámara anecoica con un fantoma de brazo de hueso animal, gel balístico y piel de cerdo. Los resultados mostraron que Wi-Fi tuvo los niveles de absorción más altos, pero estos valores (0.168 mW y 0.050 mW) estuvieron por debajo de los límites de seguridad de ICNIRP, indicando que no representaban un riesgo significativo para la salud humana.**

Palabras Claves—**Potencia de absorción, Wi-Fi, LTE, modulación AM, SAR, ICNIRP 2020.**

I. INTRODUCTION

THE 1 to 5 GHz spectrum supports wireless technologies such as Bluetooth, IrDA, UWB, Wi-Fi, and Zigbee. Bluetooth connects peripherals, IrDA enables point-to-point data transfer, Zigbee is used for process tracking, and UWB provides high-bandwidth links. These technologies are essential for modern connectivity and are categorized into Personal, Local, Metropolitan, and Wide Area Networks based on their application and range [1]. Wireless networks can be divided into short-range and long-range segments. Short-range wireless networks, such as Local Area Networks (LAN) and Personal Area Networks (PAN), operate in confined areas like corporate buildings, campuses, factories, and homes, typically using the unlicensed ISM band reserved for industrial, scientific, and medical use [2].

Radiation in the human body refers to exposure to electromagnetic radiation from wireless devices, which can affect health. Clinical studies have shown that overexposure to

subatomic particles in radiation waves can negatively affect health [3]. The effects range from tissue heating to potential long-term impacts on physical well-being. Therefore, IEEE 802.15.6 standards specify three transmission mediums: Human Body Communication (HBC) PHY, which uses the human body for signal propagation; Narrow Band (NB) PHY; and Ultrawideband (UWB) PHY. The UWB PHY operates in either a low-frequency band (3.1 to 4.8 GHz) or a high-frequency band (6 to 10.6 GHz) [4], [5]. The ICNIRP 2020 guidelines set maximum exposure levels and specific absorption rate (SAR) limits to safeguard individuals from adverse health effects of electromagnetic fields (EMF). The SAR limit is 2 W/kg for general public exposure, averaging over 10 grams of tissue [6]. The guidelines distinguish between frequencies below and above 6 GHz, recommending SAR limits of 2 W/kg for the head and trunk, 4 W/kg for limbs, and 10 W/kg for occupational exposure. For frequencies above 6 GHz, they suggest using absorbed power density to measure exposure more accurately [7].

Various techniques measure radiation in the human body: external dosimetry for surface measurements and internal dosimetry for assessing internal exposure to radioactive materials. Positron Emission Tomography (PET) and Nuclear Magnetic Resonance (NMR) provide detailed internal images without ionizing radiation, advancing our understanding of radiation exposure. In Cuenca, Ecuador, a study used Specific Absorption Rate (SAR) to quantify electromagnetic field interaction, measuring power absorbed per kilogram of tissue from 100 KHz to 10 GHz [8]. For biological tissues, the permittivity varies with the tissue type and the electromagnetic field frequency. The most commonly referenced values come from data collected at various frequencies for tissues like muscle, fat, skin, brain, etc. [9]. Assuming the tissue is a muscle, a standard reference for SAR calculations in limbs, the permittivity can be approximated using standard references [10].

This study investigates the absorption of radiation power by the human body using three Vivaldi antennas operating from 1 GHz to 5 GHz. Measurements were conducted in an anechoic chamber with a homemade arm phantom made of animal bone, ballistic gel, and pigskin, simulating skin, fat, muscle, and bone layers. Two scenarios were compared: Case 1, the system calibration, and Case 2, with the arm phantom. The objective of utilizing Wi-Fi, LTE technologies, and AM

Cruz Jenny, Ñaupa Alex, and Silva Belén are with the Facultad de Informática y Electrónica, Escuela Superior Politécnica de Chimborazo, Riobamba, Ecuador (e-mail: {jenny.cruz, alex.naupa, belen.silva}@espoch.edu.ec).

modulation is to determine how much radiation power the human body absorbs and how this varies with frequency and distance.

II. THEORETICAL FRAMEWORK

A. Anatomy of the Human Arm

The anatomy of the arm is fascinating and complex, composed of muscles, bones, joints, blood vessels, and nerves that work harmoniously to allow a wide range of movements and functions. The arm is designed for mobility, strength, and agility from the shoulder to the elbow, essential for everyday activities and more demanding physical tasks [11]. The arm is the second segment of the upper limb and articulates with the first at the shoulder and the second at the elbow, thus connecting the shoulder to the forearm [12]. The region that contacts the trunk is the shoulder girdle, formed by the clavicle and the scapula. The latter connects to the upper limb through the shoulder joint. The humerus is the only bone in the arm (strictly speaking) Fig.1. In the proximal humerus, the muscles responsible for the movements of the shoulder joint insert, allowing its excellent mobility, while the muscles responsible for the mobility of the elbow originate in the distal part of the humerus [13].

B. Materials that simulate the composition of muscle and human skin include

For many years, ballistic tests have been conducted on pieces of animal meat to compare their effects on human flesh. However, the cost of maintaining the meat due to its decomposition and the repetitiveness of the tests led to the development of a synthetic material that could mimic human skin [14].

Due to this need, ballistic gel is created. It simulates human tissues and muscles, possessing similar mechanical characteristics, as water constitutes a significant proportion of both. It is mainly composed of water and gelatin, which provides the density and viscosity that allow it to mimic human tissue [15].

C. Phantoma

Phantoms or mannequins are devices whose shape and material simulate human body characteristics. They are used in quality assurance procedures and strategies to optimize the balance between dose and image quality [16]. Biological phantoms play a significant role in the use and development of medical technologies for diagnosing, treating, and characterizing tissues and biological fluids [17].

D. Utility of the Human Phantom

Phantoms are fundamental tools in the research and development of medical devices. These anatomical models accurately reproduce the structure and characteristics of certain human body parts, allowing for testing and experiments in a controlled and safe environment. Their utility extends to biomechanics, biomedical engineering, and medical simulation, thus contributing to innovative solutions and refining clinical skills [18]. A phantom is essential for guiding instrumentation development and characterizing its specifications and performance. They also allow for the calibration of measurement and diagnostic equipment before their use on humans or animals, providing the equipment with more excellent safety. Most importantly, phantoms serve as training instruments for users who need to operate measurement and diagnostic equipment in a safe environment, free from the pressure of the consequences resulting from possible errors during this learning phase [19].

III. METHODOLOGY

The implemented system uses two stages: the first stage is calibration, which refers to the transmitter-receiver system, as shown in Fig. 2, and the second stage focuses on taking measurements in the anechoic chamber, as depicted in Fig. 3.
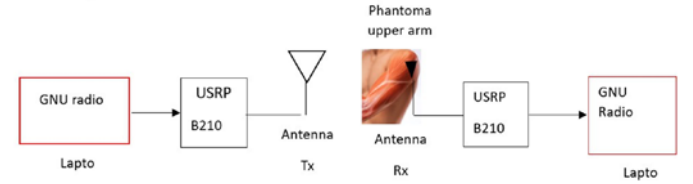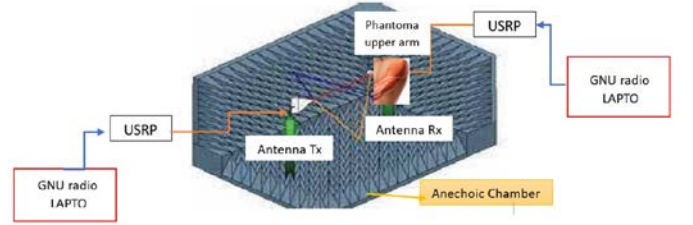

Fig. 1. Butler matrix structure.

Fig. 2. Measurement System.

A. Transmitter System

The transmitter system was designed using GNU Radio, a signal processing and software-defined radio (SDR) software that provides a flexible and powerful platform for designing and executing communication systems. GNU Radio's modulation is amplitude modulation (AM), which involves modulating the amplitude of a high-frequency carrier wave with the desired information.

The transmission system comprises the generation of two signals: a baseband information signal, which operates around the origin, and a carrier signal, with a high operating frequency. Each of these signals has a modulating and carrier amplitude, respectively. Both signals are multiplied and summed, resulting in a passband-type signal.

Frequencies high enough to efficiently radiate from an antenna and propagate through free space are typically called radio frequency (RF). The information acts on the RF carrier in the modulator and produces a modulated waveform.

The above-described process was designed in GNU Radio to obtain an amplitude-modulated (AM) signal. Fig. 4 shows the configuration of each process in blocks.
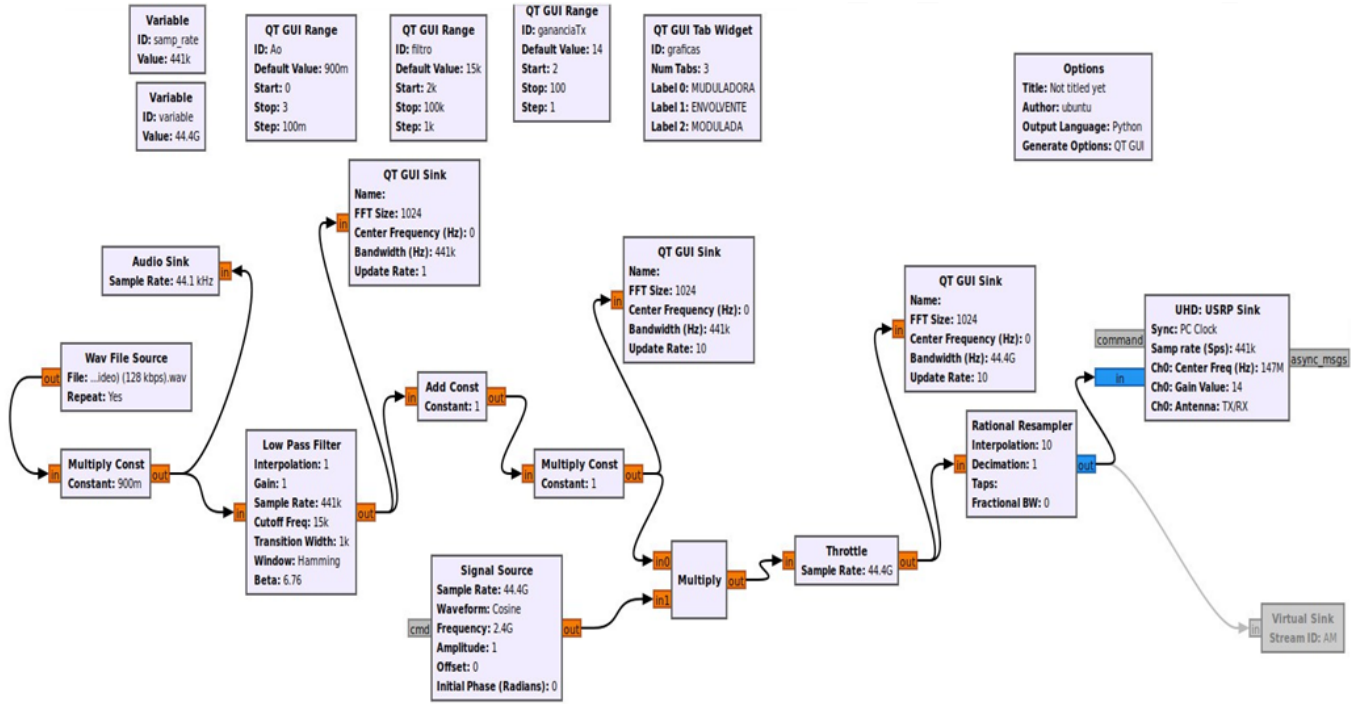
Fig. 3. UPNa microgrid configuration, components description and bus connections.

In amplitude modulation (AM), the amplitude of the carrier signal varies according to the amplitude of the information signal. In this case, the frequency of the information signal is 147 KHz (0.147 MHz), and the frequency of the carrier signal is 2.5 GHz (2500 MHz). In the time domain, the waveform of the carrier signal is observed oscillating at a frequency of 2.5 GHz, and the information signal modulates this amplitude. The modulated AM signal would have a central frequency of 2.5 GHz, and the information signal would determine the variations in the amplitude of this signal.

B. Sensory System

An AM receiver flowchart designed in GNU Radio is presented. The process begins with the AM signal received by an antenna and passed to a USRP Source block, configuring the USRP device to receive and convert the AM signal into digital data. This digital signal is then sent to a Band Pass Filter block to remove unwanted frequencies, with cutoff frequencies set slightly below and above the AM carrier frequency.

Next, the filtered signal is passed to a multiplied block, multiplied by a sinusoidal signal of the same frequency as the AM carrier, resulting in the complex envelope signal. This signal is then passed through a Low Pass Filter block to remove high frequencies, with the filter's cutoff frequency set much lower than the AM carrier frequency.

A complex floating block converts the filtered low-pass signal into a real-magnitude signal, producing the demodulated audio signal containing the original transmitted information. This process, designed in GNU Radio to retrieve the original information signal, is depicted in Fig. 4.

The implemented system will test two commonly used technologies: LTE, represented by a cell phone (Fig. 5), and Wi-Fi, represented by a router (Fig. 6).
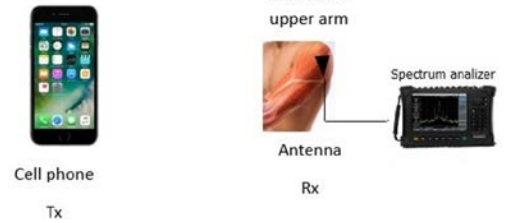

Fig. 4. LTE Tx and Rx Diagram.

The LTE signal is generated at the cell phone tower and transmitted over the air to the cell phone. The bowtie antenna in the receiver receives the signal and converts it into an electrical signal, which will be processed in the USRP to extract the transmitted information. This information can be stored in a file or displayed on a screen. It will be displayed on the laptop using the GNU Radio graphical interface.
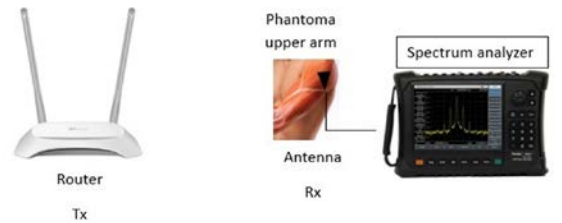

Fig. 5. Tx and Rx diagram of WI-FI technology.

The process begins with the router generating the Wi-Fi signal. The router receives data from the Internet through an

Ethernet cable or a wireless connection, encodes the data into a Wi-Fi signal, and transmits it through its monopole antennas.

The bowtie antenna, attached to the phantom arm, receives the Wi-Fi signal and converts it into an electrical signal.

The spectrum analyzer analyzes the Wi-Fi signal received by the bowtie antenna. It can display signal strength, frequency, and bandwidth, which can be used to measure the intensity of power absorbed by the arm.

IV. Design Of The Human Arm Phantom

The design of the human arm phantom involves careful planning to balance anatomical accuracy and functionality. Beginning with a detailed analysis of the human arm's anatomy, key structures to be replicated in the model are identified. From there, the design includes selecting suitable materials to replicate human tissue's texture and biomechanical properties. Features are also integrated to allow for modification and adaptation of the phantom for different purposes, such as inserting medical devices or simulating specific procedures.

A. Design in Zygote Body

Design Parameters for the Arm Phantom:
- Humerus Length: 19 cm
- Humerus Thickness: 4 cm
- Scapula Length: 16 cm
- Scapula Height: 13 cm
- Scapula Thickness: 1.5 cm

Next, a layered 3D design of the arm phantom is generated in the Zygote Body simulator, as depicted in Fig. 7, Fig. 8, and Fig. 9.

Fig. 6. Skeletal system of the arm, frontal and posterior.

Fig. 7. Muscular system of the arm, frontal and posterior.

Fig. 8. Dermatological system of the arm, frontal and posterior.

The structure will be generated for subsequent implementation with varnished animal bones and ballistic gel.

V. Construction Of The Human Arm Phantom

The construction of a human arm phantom is a meticulous process that requires a combination of anatomy, engineering, and knowledge of specialized materials. To create an accurate and functional model, three-dimensional scanning techniques are used to capture the human arm's morphology precisely. Then, silicone, resins, and synthetic tissues replicate human tissue's texture and biomechanical characteristics. In addition, internal structures simulating bones, muscles, and blood vessels are integrated, providing anatomical realism to the phantom. This construction process is carried out with a focus on anatomical fidelity and functionality, allowing the phantom to be an effective tool in research, education, and the development of medical devices.

A. Ballistic Gel Construction

To make the ballistic gel (in its original composition), the following ingredients were used:
- 3 or 5 tablespoons of neutral gelatin (in two different quantities to check how its properties vary)
- one tablespoon of glycerin soap
- one tablespoon of vinegar
- three tablespoons of homemade glue or gum arabic
- 500 ml of water

The manufacturing process consists of 2 steps: first, all the ingredients were mixed in very hot water (without reaching boiling point), and then the mixture was allowed to rest either in the refrigerator or freezer to study how the properties vary depending on the cooling rate. White glue was added to the mixture for the two variants made to see if they could provide any interesting properties to the material.

B. Construction of the Phantom Layers

In this study, three distinct layers were used to construct the arm phantom, aiming to simulate the absorption of electromagnetic waves by human tissues realistically. The composition and purpose of each layer are described below:
1) *First Layer: Skin and Fat:*
   - Composition: Pigskin.
   - Purpose: Simulate human skin and subcutaneous fat, using pigskin for its similar physical and dielectric properties.
2) *Second Layer: Skin, Fat, and Muscle*
   - Composition: Pigskin and homemade ballistic gel.
   - Purpose: To simulate skin, fat, and muscle, ballistic gel

mimics muscle tissue for a more complete representation.

3) *Third Layer: Skin, Fat, Muscle, and Bone*
- Composition: Pigskin, homemade ballistic gel, and animal bone.
- Purpose: Simulate skin, fat, muscle, and bone, with animal bone providing an accurate representation of internal structures and their effect on electromagnetic wave absorption.

Fig. 9. Arm model: Separate Layers.

Fig. 10 shows each of the three layers (pigskin, ballistic gel, and animal bone) separately, highlighting the materials used and the structure of each layer.
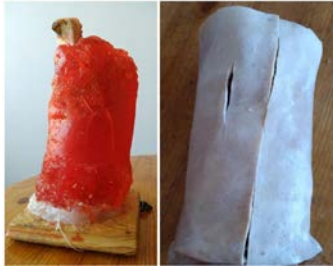

Fig. 10. Arm model: Combined Layers.

Fig. 11 shows the layers combined to form the complete arm phantom. It demonstrates how the layers were assembled to mimic the structure of the human arm: skin, fat, muscle, and bone. Table 1 summarizes the conformation of each layer of the arm phantom.

TABLE I
CONFORMATION OF THE DIFFERENT LAYERS

Layers	Skin	Fat	Muscle	Bone
1	X	X		
2	X	X	X	
3	X	X	X	X

VI. DESIGN OF THE VIVALDI ANTENNA

Vivaldi antennas are a type of broadband slot antenna known for their exceptional bandwidth, spanning multiple octaves. Their design consists of a conical slot etched into a dielectric substrate. The slot's conical shape gradually increases the antenna impedance as it moves away from the vertex, allowing the antenna to operate over a wide range of frequencies.

A. Parametric Equations

Parametric equations for the design of the Vivaldi antenna can be expressed in terms of sine and cosine functions using fundamental trigonometric relationships. This allows for a more intuitive representation of the slot shape and facilitates its analysis and visualization.

B. General equation

The general equation for the Vivaldi groove shape in polar coordinates (r, θ) can be expressed as:
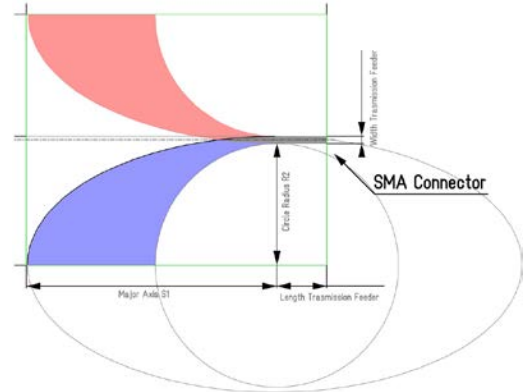

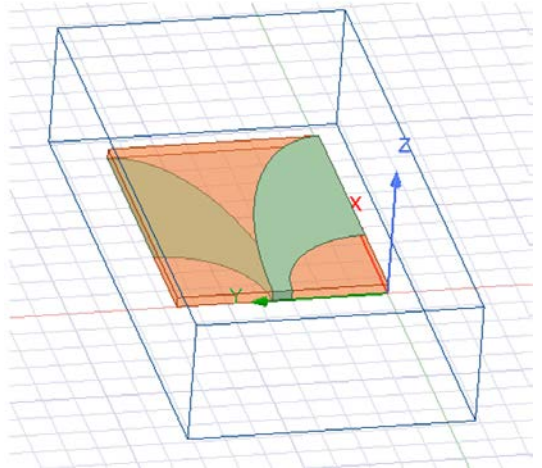Fig. 11. Parametric Equations: Eclipse and Circle.

Fig. 12. Vivaldi antenna design in HFSS.

In Fig. 12, we can see how the parametric equations of the ellipse and the circle are used to design the Vivaldi antenna.

$$x = S1 \cdot \cos(\theta) \quad (1)$$

$$y = R1 \cdot \sin(\theta) \quad (2)$$

where x and y are the parametric equations of the ellipse, $S1$ is the major radius of the ellipse, and $R1$ is the minor radius of the ellipse.

$$x = R2 \cdot \cos(\theta) \quad (3)$$

$$y = R2 \cdot \sin(\theta) \quad (4)$$

where x and y are the parametric equations of the circle, and $R2$ is the circle's radius.

C. Typical values

Typical values for parameters $R2$ and $S1$ in Vivaldi antenna design in terms of sine and cosine are:

$$R2 = R1 - width\ transmision\ feeder$$
$$S1 > R1 \tag{5}$$

D. Simulation of Vivaldi Antenna

Vivaldi antennas, known for their wide bandwidth and simple design, find applications in various areas of wireless communications. In this work, Vivaldi antennas will be designed and simulated using Ansys HFSS software for the frequencies of the three technologies. The results, such as radiation pattern, bandwidth, and efficiency, will be analyzed and discussed later.

Fig. 13 shows the design for the four Vivaldi antennas operating in a different frequency band in HFSS.

Fig. 13. Implementation of Vivaldi antennas 1.1, 1.2, and 1.3.

As shown in Fig. 14, three Vivaldi receiving antennas, labeled 1.1, 1.2, and 1.3, were implemented. Their respective bandwidths were (4 to 5.88) GHz, (1.67 to 3.64) GHz, and (2.77 to 5.28) GHz.
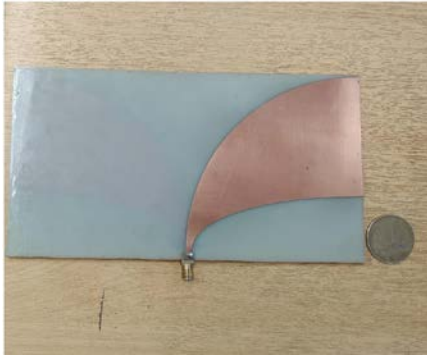

Fig. 14. Transmitting Vivaldi antenna 1.4.

As shown in Fig. 15, this transmitting antenna is designed for measurements using USRP modules, which transmit an AM-modulated signal. This signal will be measured in the various layers of the phantom and without it. The antenna operates in the frequency band from 1.50 GHz to 5.19 GHz and has a bandwidth of 3.69 GHz.
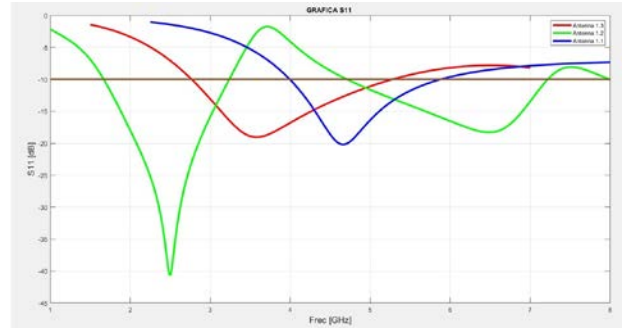

Fig. 15. Reflection coefficient S11 of the Vivaldi receiving antenna.

VII. RESULTS

A. Reflection Coefficient and Radiation Pattern of the Receiving Antennas

As shown in Fig. 16, the reflection coefficient results for the Vivaldi receiver antennas 1.1, 1.2, and 1.3 were presented. The total bandwidth covered by these antennas ranged from approximately 1.67 GHz to 5.88 GHz.

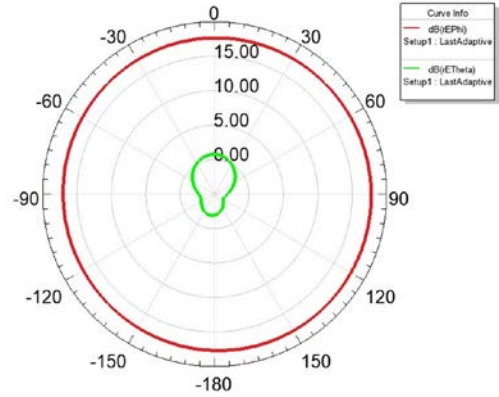Fig. 16. Radiation pattern of the Vivaldi antenna 1.1.

In Fig. 17, we can see the radiation pattern of the Vivaldi antenna, which exhibits higher radiation at 0 degrees and decreases as it approaches 90 degrees.
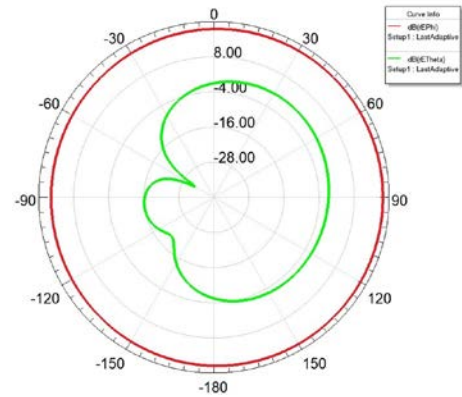

Fig. 17. Radiation pattern of the Vivaldi antenna 1.2.

Fig. 18 shows the Vivaldi antenna's radiation pattern, showing higher radiation at 90 degrees and decreasing as it approaches zero.
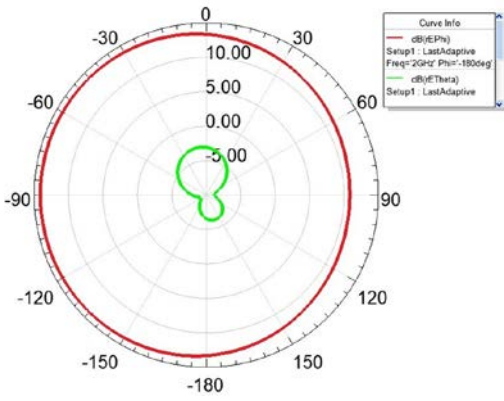
Fig. 18. Radiation pattern of the Vivaldi antenna 1.3.

Fig. 19 shows the radiation pattern of the Vivaldi antenna, which shows higher radiation at -15 degrees and decreases as it approaches 90 degrees.
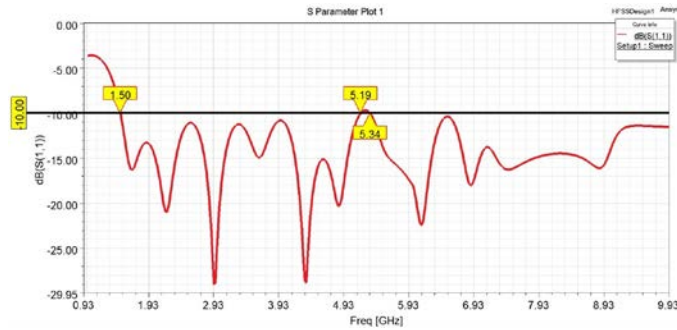

Fig. 19. Reflection coefficient S11 of the Vivaldi antenna 1.4.

B. Simulation of antenna 1.4

In Fig. 20, it was observed that the Vivaldi transmitting antenna 1.4 operated in a frequency range from 1.50 GHz to 5.19 GHz, with a bandwidth of 3.66 GHz

Fig. 21 shows the radiation pattern of the Vivaldi transmitting antenna 1.4. It is directive, with the highest amount of radiation at 90 degrees and decreasing as it approaches 0 degrees.

The measurements were conducted inside an experimental anechoic chamber provided by the Faculty of Computer Science and Electronics. The arm phantom, antenna mounts, an internet router, and a cellular phone were positioned to conduct measurements within this chamber under various conditions and distances.
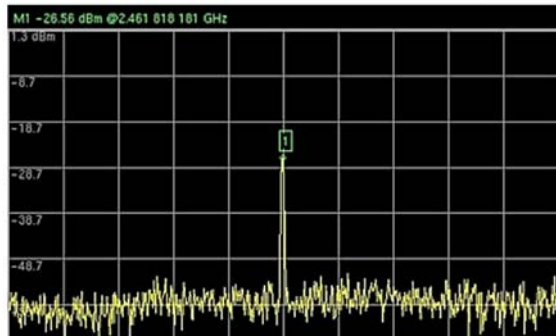

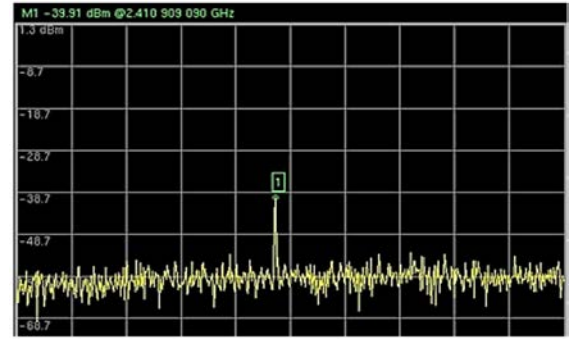Fig. 20. Calibration of the system for Wi-Fi technology at 80 cm.

Fig. 21. Wi-Fi Antenna Measurement 1.3 at 80 cm in phantom layer 3.

C. Case 1: System calibration

It used a router connected directly to the ESPOCH DNS as a repeater for Wi-Fi technology to conduct the radiation power measurements for system calibration and the measurements using the phantom. For LTE technology, it uses a mobile phone. Finally, AM modulation measurements used a USRP connected to a computer running GNU Radio at a transmission frequency of 3.09 GHz.

For the calibration of the measurements, three types of technologies were subjected to the same conditions: distance, height, and location in the same scenario (anechoic chamber), as well as frequency, depending on the type of technology. Parameters such as the distance between the Tx antenna and the phantom, the height between the ground and the Rx antenna position, which is 40 cm for all cases, and the position of the Rx antenna and the location point of the Rx antenna on the arm according to the radiation pattern it has in the privileged direction to obtain maximum power reception were taken into account, where the main lobe was directed downwards, that is, along the -Z axis.

TABLE II
CALIBRATION OF THE TECHNOLOGY

Antenna	Frequency (GHz)	Distance (cm)	Power (dBm)
Wi-Fi technology			
1.1	2.45	80	-25.62
1.2	2.45	80	-35.36
1.3	2.46	80	-31.31
LTE technology			
1.1	1.9	18	-31.58
1.2	1.9	18	-30.72
1.3	1.9	18	-29.60
1.1	1.9	60	-50.69
1.2	1.9	60	-33.36
1.3	1.9	60	-31.72
USRP technology			
1.1	3.08	24	-20.87
1.2	3.08	24	-30.46
1.3	3.08	24	-24.36

According to Table II, the system calibration for Wi-Fi technology at a distance of 80 cm resulted in relatively high power levels for the three Rx antennas. The antenna that demonstrated the most efficient response was antenna 1.1 with -25.62 dBm, followed by antenna 1.3 with -31.31 dBm, and finally, antenna 1.2 with a response of -35.36 dBm.

The results using LTE technology at a distance of 18 cm show that antenna 1.3 delivered the best result with -29.60 dBm, followed by antenna 1.2 with a received power of -30.72

dBm, and finally, antenna 1.1 with a power of -31.58 dBm. The same technology at a distance of 60 cm shows that the antenna with the best-received power was 1.3 with -31.72 dBm, followed by antenna 1.2 with -33.36 dBm, and finally, antenna 1.1 with a received power of -50.69 dBm.

The system calibration for AM modulation was transmitted using a USRP with GNU Radio and Antenna 1.4 (Tx). At a distance of 24 cm, antenna 1.1 had the best response, with a received power of -20.87 dBm. This was followed by antenna 1.3, with a power of -24.36 dBm, and finally, antenna 1.2, with a power of -30.46 dBm.

These results were essential for establishing a baseline for comparing and analyzing the measurements within the phantom, considering that the frequencies change according to the technology in each case.

D. Case 2: Measurements inside the phantom

The second measurement case used a homemade human arm phantom composed of different layers simulating the texture of an accurate arm. Based on Table I, they conducted multiple measurements on the phantom's various layers to analyze the radiation's power absorption in each layer.

TABLE III
WI-FI TECHNOLOGY MEASUREMENTS IN PHANTOM LAYERS AT 80 CM

	Frequency (GHz)				Power (dBm)		
	Ant 1.1	Ant 1.2	Ant 1.3		Ant 1.1	Ant 1.2	Ant 1.3
1	2.45	2.45	2.45		-25.90	-36.92	-38.34
2	2.45	2.46	2.45	80	-31.47	-39.98	-44.97
3	2.41	2.41	2.41		-31.76	-47.51	-48.31

For Wi-Fi technology, the router was set up, and the first layer of the phantom was placed at a distance of 80 cm. According to Table III, the results for antenna 1.1 were 2.45 GHz, with a significant decrease in power between the first layer and layer number 3. The total power decrease was -5.86 dBm. For antenna 1.2, the power decrease between the first and third layers was -10.59 dBm, and finally, for antenna 1.3, the power decrease between the first and third layers was -9.97 dBm.

TABLE IV
LTE TECHNOLOGY MEASUREMENTS IN PHANTOM LAYERS AT 18 CM

	Frequency (GHz)				Power (dBm)		
	Ant 1.1	Ant 1.2	Ant 1.3		Ant 1.1	Ant 1.2	Ant 1.3
1	1.9	1.9	1.9		-52.44	-35.99	-39.14
2	1.9	1.9	1.9	18	-59.48	-57.73	-46.93
3	1.9	1.9	1.9		-	-57.81	-48.43

For LTE technology, a cellphone with a frequency of 1.9 GHz was placed at a distance of 18 cm. According to Table IV, the results for antenna 1.1 showed a significant decrease in power between the first and second layers, with a total power decrease of -7.04 dBm. For antenna 1.2, the power decrease between the first and third layers was -21.82 dBm, and finally, for antenna 1.3, the power decrease between the first and third layers was -9.29 dBm.

TABLE V
LTE TECHNOLOGY MEASUREMENTS IN PHANTOM LAYERS AT 60 CM

	Frequency (GHz)				Power (dBm)		
	Ant 1.1	Ant 1.2	Ant 1.3		Ant 1.1	Ant 1.2	Ant 1.3
1	1.9	1.9	1.9		-55.67	-36.11	-34.55
2	1.9	1.9	1.9	60	-62.91	-55.66	-51.52
3	1.9	1.9	1.9		-	-63.09	-63.90

For LTE technology, a cellphone with a frequency of 1.9 GHz was placed at a distance of 60 cm. According to Table V, the results for antenna 1.1 showed a significant decrease in power between the first and second layers, with a total power decrease of -7.24 dBm. For antenna 1.2, the power decrease between the first and third layers was -26.98 dBm, and finally, for antenna 1.3, the power decrease between the first and third layers was -29.35 dBm.

As detailed in Table VI, the measurements using USRP with AM modulation at 3.08 GHz showed varying received power levels across the layers. Layer 1's signals were generally strongest, particularly with antenna 1.2. In Layer 2, the power levels were slightly lower but still showed better performance with antenna 1.2. Layer 3 exhibited the most significant signal attenuation, significantly affecting antenna 1.1, indicating a substantial decrease in signal penetration through more complex layers. These results highlight the impact of the layer composition on signal reception, with more complex structures leading to higher signal loss.

TABLE VI
USRP TECHNOLOGY MEASUREMENTS IN PHANTOM LAYERS AT 24 CM

	Frequency (GHz)				Power (dBm)		
	Ant 1.1	Ant 1.2	Ant 1.3		Ant 1.1	Ant 1.2	Ant 1.3
1	3.08	3.08	3.08		-37.33	-33.07	-38.6
2	3.08	3.08	3.08	24	-39.83	-33.84	-39.17
3	3.08	3.08	3.08		-57.48	-45.27	-45.89

E. Comparison of absorption power between different technologies

To conduct measurements of absorbed power according to the ICNIRP 2020 standard, a relative permittivity of 52 and a conductivity of approximately 1.73 S/m were used for Wi-Fi technology at a frequency of 2.5 GHz. For LTE technology at a frequency of 1.9 GHz, relative permittivity values of 55 and a conductivity of 1.0 S/m were utilized; for AM modulation at a frequency of 3.08 GHz, a relative permittivity of 49 and a conductivity of approximately 2.2 S/m were employed. These values were derived from typical dielectric properties of biological tissues, which can vary slightly based on specific conditions and measurement methods [6], [7].

Fig. 22 shows that the power decreased using antenna 1.2, which operated within a band from 1.67 GHz to 3.24 GHz, as specified in Table II. At the same time, measurements were taken in different layers of the phantom. For Wi-Fi technology, a notable decrease in power was observed from the free-space measurement of -35.36 dBm to the last layer of the phantom at -47.51 dBm, indicating an absorption of -12.15 dBm. When converted to the Specific Absorption Rate (SAR) at 2.45 GHz, this measurement yielded a power distribution of approximately 0.168 mW. According to the ICNIRP SAR

limit for general public exposure (2 W/kg), this level is within safe limits.

For LTE technology at 1.9 GHz, at a distance of 18 cm, power decreased from -31.58 dBm in free space to -57.81 dBm in the last layer of the phantom, indicating an absorption of -26.23 dBm. The corresponding SAR measurement yielded approximately 0.0058 mW, significantly below the safety limit.

For AM modulation at 3.09 GHz and the same distance, power decreased from -30.46 dBm in free space to -45.27 dBm in the last layer of the phantom, indicating an absorption of -14.81 dBm. This SAR measurement yielded approximately 0.030 mW, also within safe limits.
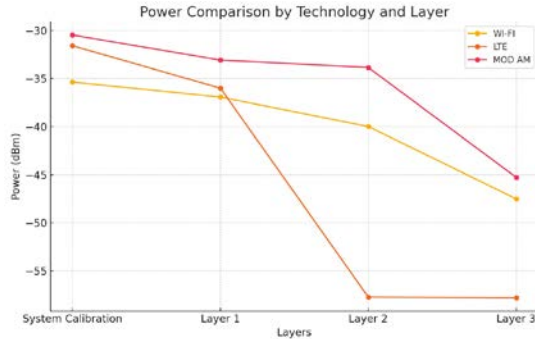

Fig. 22. Power Comparison for Antenna 1.2.

According to Fig. 23, using antenna 1.3, which operated in a band from 3.60 GHz to 5.90 GHz, as specified in Table II, a progressive decrease in power was observed as the layers of the phantom increased.

For Wi-Fi technology at 2.5 GHz, power decreased from -31.31 dBm in free space to -48.31 dBm in the last layer of the phantom, indicating an absorption of -17 dBm. This measurement converted to Specific Absorption Rate (SAR) yielded a power distribution of approximately 0.050 mW, resulting in a SAR of 0.02 mW when absorbed by 2 kg of tissue. This value is significantly lower than the permissible levels, indicating that the absorption is not harmful.

For LTE technology at 1.9 GHz and a distance of 18 cm, power decreased from -29.60 dBm in free space to -48.43 dBm in the last layer of the phantom, indicating an absorption of -21.83 dBm. This measurement yielded a SAR of 0.0066 mW when absorbed by 2 kg of tissue, which is well below the safety limit, indicating no harm.

For AM modulation at 3.09 GHz and the same distance, power decreased from -24.36 dBm in free space to -45.89 dBm in the last layer of the phantom, indicating an absorption of -21.53 dBm. This measurement yielded a SAR of 0.015 mW when absorbed by 2 kg of tissue, which was also within safe limits.
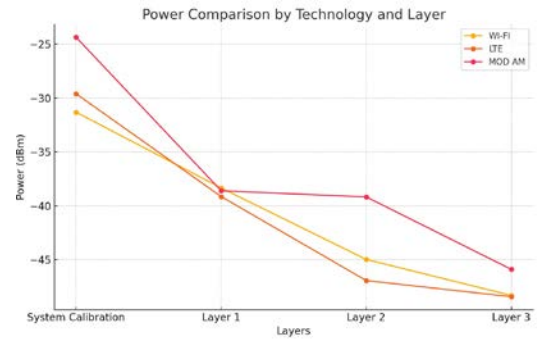

Fig. 23. Power Comparison for Antenna 1.3.

VIII. CONCLUSIONS

The study found that Wi-Fi exhibited the highest absorption levels at 0.168 mW and 0.050 mW, and AM modulation had the lowest absorption levels, with values of 0.015 mW and 0.030 mW. However, these values remained within the safety limits set by ICNIRP 2020 for SAR (Specific Absorption Rate) and power density [20]. As a result, the radiation absorbed from the tested technologies posed no significant risk to human health.

REFERENCES

[1] S. Ullah, H. Higgins, B. Braem, et al., "A Comprehensive Survey of Wireless Body Area Networks," *Journal of Medical Systems*, vol. 36, pp. 1065-1094, Aug. 2010.

[2] J. Salazar, Redes Inalámbricas, "Thesis, České vysoké učení technické v Praze, Fakulta elektrotechnická, Praha, Czech Republic, 2022. [Online]. Available: https://upcommons.upc.edu/bitstream/handle/2117/100918/LM01-R-ES.pdf.

[3] R. Sánchez, K. Buri, S. Sarango, C. Cabrera, "Avances tecnológicos y científicos en radiología," *Avances tecnológicos y científicos en radiología. RECIAMUC*, vol. 7, pp. 457-465, Abr. 2023.

[4] J. P. Michelino, "Performance de IEEE 802.15.6 en coexisten- cia con IEEE 802.15.4 e IEEE 802.11,"Thesis, Universidad Nacional de La Plata, Facultad de Informática, December 2020.

[5] S. Ullah, M. Mohaisen, M. A. Alnuem, "A review of IEEE 802.15.6 MAC, PHY, and security specifications," *International Journal of Distributed Sensor Networks*, pp. 1-12, Apr. 2013.

[6] International Commission on Non-Ionizing Radiation Protection (IC-NIRP), "ICNIRP Guidelines for Limiting Exposure to Electromagne- tic Fields (100 kHz to 300 GHz)," 2020. [Online]. Available: https://www.icnirp.org/cms/upload/publications/ICNIRPrfgdl2020.pdf. [Accessed: 26-Jul-2024].

[7] International Commission on Non-Ionizing Radiation Protection (IC-NIRP), "Specific Absorption Rate (SAR)," [Online]. Available: https://www.icnirp.org/en/frequencies/sar.html.[Accessed:26-Jul-2024].

[8] D. M. Andrade Guerrero y C. F. Contreras Ortiz, "Medición y análisis del nivel de exposición a radiaciones no ionizantes (RNI) en ambientes indoor en la ciudad de Cuenca, dentro del espectro radioeléctrico en la banda de frecuencia de telefonía celular," Tesis de la Universidad Politécnica Salesiana, Cuenca, Ecuador, 2014.

[9] IT'IS Foundation, "Tissue Properties Database," [Online]. Available: https://itis.swiss/virtual-population/tissue-properties/database/. [Accessed: 26-Jul-2024].

[10] IT'IS Foundation, Çustomized Research: Tissue Models Database,"[Online]. Available: https://itis.swiss/customized-research/tissue-models-database/. [Accessed: 26-Jul-2024].

[11] S. Pardo Alia, "Control del brazo robot irb120 mediante el dispositivo háptico phantom," 2016. [Online]. Available: https://ebuah.uah.es/dspace/handle/10017/26467.

[12] E. Peréz, "Enlace de Comunicación," May. 2023. [Online]. Available: https://repositorio.unbosque.edu.co/server/api/core/bitstreams/ea76f11b-7dfe-498b-9d48-9d6b7398e0a2/content. [Accessed: Apr. 19, 2024].

[13] J. Pipa,"Google Scholar,"2019. [Online]. Available: https://gc. scalahed.com/recursos/files/r161r/w25923w/S5R1.pdf. [Accessed: Apr. 19, 2024].

[14] E. Peréz, "Antena implantable a 2.45 GHz para telemetría biomédica implementada al interior de liquidos equivalentes de tejido (musculo, grasa y piel) y/o geles de imitación (phantom), Universidad el Bosque, Facultad de Ingeniería, May. 2023.

[15] N. Palomar, "Diseño de antenas UWB directivas y tamaño compacto para aplicaciones médicas operando en el entorno corporal," Jul. 2019. [Online]. Available:https://1library.co/document/

[16] A. Calderón, L. Arce y R. Mejías, "Control de calidad de imagen y dosimetría, para mamografía digital, utilizando el fantoma Normi Mam Digital," *Uniciencia*, vol. 32, no.2, pp. 70-81, Dec. 2018.

[17] F. Chinchurreta and R. Shaporin, "Fantomas y símiles de tejidos para aplicaciones biomédicas, [Online]. Available: https://www.itefi.csic.es/es/daend/ulab/fantomas-y-similes-de-tejidos-para-aplicaciones-biomedicas. [Accessed: Apr. 19, 2024].

[18] L. Pérez, "Anatomía evolutiva de brazo y el antebrazo en los homininos, Tesis Universidad Complutense de Madrid, 2017.

[19] "Las personas pasan conectadas más de un cuarto del día," Ecuador Verifica, Jun. 2, 2022. Available: https://ecuadorverifica.org/2022/06/02/las-personas-pasan-conectadas-mas-de-un-cuarto-del-dia/. [Accessed: Jul. 26, 2024].

DEPARTAMENTO DE ELÉCTRICA, ELECTRÓNICA Y TELECOMUNICACIONES
Universidad de las Fuerzas Armadas – ESPE

El Departamento de Eléctrica, Electrónica y Telecomunicaciones (antigua Facultad de Ingeniería Electrónica) fue creado el 25 de abril de 1977 e inicia sus labores en octubre del mismo año en la modalidad presencial, con sus planes y programas de estudio encaminados a la formación del Ingeniero Electrónico. A partir de octubre de 1990, ofrece dos carreras con perfiles profesionales definidos: Ingeniería Electrónica en Telecomunicaciones e Ingeniería Electrónica en Computación.

En la propuesta actual del Departamento se integran en un sólo perfil estas aspiraciones, ofreciendo las carreras de Ingeniería en Electrónica y Telecomunicaciones, e Ingeniería en Electrónica, Automatización y Control.

Además oferta los siguientes programas de posgrado: **Maestría de Investigación en Electrónica menciones en Automática y Telecomunicaciones**, Maestría en Redes de Información y Conectividad, y Maestría en Gerencia de Redes y Telecomunicaciones.

The Department of Electrical, Electronics, and Telecommunications (formerly the Faculty of Electronic Engineering) was created on April 25, 1977, and began its work in October of the same year in the face-to-face modality, with its study plans and programs aimed at the training of the Electronic Engineer. Since October 1990, it has offered two careers with defined professional profiles: Electronic Engineering in Telecommunications and Electronic Engineering in Computing.

The Department's current proposal integrates these aspirations into a single profile, offering the careers of Electronics and Telecommunications Engineering, and Electronics, Automation and Control Engineering.

It also offers the following graduate programs: **Research Master's in Electronics with mentions in Automation and Telecommunications**, Master's in Information Networks and Connectivity, and Master's in Network and Telecommunications Management.

Mayor información en `http://deee.espe.edu.ec/`
Further information `http://deee.espe.edu.ec/`